Characterizing Storm-Induced Coastal Flooding Using SAR Imagery and Deep Learning

Deanna Edwing, Lingsheng Meng, Suna Lv, and Xiao-Hai Yan

***Abstract*—Flooding is among the most common yet costly worldwide annual disasters. Previous studies have proven that synthetic aperture radar (SAR) is an effective tool for flooding observation due to its high-resolution and timely observations, and deep learning-based models can accurately extract water bodies from SAR imagery. However, many previous flood analyses do not account for influences of tides and permanent water bodies, and the comprehensive characteristics of coastal storm flooding are still not fully understood. This study therefore presents a novel approach for isolating storm-induced flood waters in coastal regions from SAR imagery through the identification and removal of permanent water bodies and tidal inundation. This methodology is applied to the Delaware Bay region, with ancillary geospatial data used to determine resulting landcover impacts. Results indicate that flooding primarily impacts agricultural and marsh regions, as well as urban areas like airports and road systems adjacent to rivers or large inland bays. The sensitivity impacts of tides on flood estimates reveals that estimates significantly increase if included in analysis, highlighting the importance of their removal prior to flood identification. Finally, exploration into intense coastal storm events in the Delaware Bay region reveal the importance of storm characteristics like high water levels, wind, and precipitation in generating extreme flooding conditions. The case study presented here has important implications for other coastal regions and provides an innovative and comprehensive approach to coastal storm flood identification and characterization which can benefit coastal managers, emergency responders, coastal communities, and researchers interested in coastal flood hazards.**

***Index Terms*—Convolutional neural network (CNN), deep learning, Delaware Bay, flood mapping, image segmentation, Sentinel-1, synthetic aperture radar (SAR).**

I. Introduction

FLOODING is one of the most frequent, costly, and deadly coastal hazards facing communities every year [1], [2]. With past and ongoing changes in weather variability reshaping the environment, flooding is becoming a greater concern for coastal communities [3]. In particular, the Northeast (NE) United States is consistently identified as a region where climate change is leading to increases in coastal flooding frequency [4] and intensity [5], [6]. The risk to both local communities and the surrounding landscapes necessitates a better understanding of such events for landowner safety and coastal management. Recent works have leveraged computational approaches involving remote sensing observations and machine learning (i.e., neural networks), transforming them into powerful tools for flood-detection. By cooperatively utilizing such tools, increasingly complex and intricate questions can be answered about the spatial trends and oceanographic mechanisms of coastal flooding in localized regions.

Early water body detection relied on site-specific on-the-spot investigations which were often labor-intensive and time-dependent, making it difficult to accurately analyze wide-scale flooding. The development of remote sensing technologies like satellites addressed the need for rapid imaging response, large spatial coverage, cost-efficiency, and low-risk information extraction, thereby becoming the principal method for flood observation. There are two types of satellite sensors that can be used for flood detection, optical and microwave. Most optical sensors are passive, operating exclusively during daylight hours and in fair-weather conditions, thereby hindering their use for flood mapping since such events typically coincide with cloudy or foggy weather. Conversely, synthetic aperture radar (SAR), an active microwave sensor, can image both day and night and in near-all weather conditions; moreover, its high-resolution capabilities enable water detection with high precision. SAR is therefore highly suitable for flood detecting.

Traditional methods of flood detection from satellite imagery have included histogram thresholding [7], change detection [8], and active contouring [9]; however, the accuracy of these methods depends on many factors including the speckle of SAR imagery, user-dependent parameter tuning, and interference factors like vegetation or soil moisture that have similar backscattering characteristics to water bodies. In recent years, the use of deep learning methods such as convolutional neural networks (CNNs) in image classification have greatly decreased the processing time necessary to produce flood maps while also increasing the accuracy of extracting floodwater extent. Over the past decade, the number of papers published on the utilization of CNNs for water-body segmentation in SAR imagery has rapidly increased [10], [11], including advancements in water-land segmentation

Received 27 April 2024; revised 13 September 2024 and 5 November 2024; accepted 6 January 2025. Date of publication 21 January 2025; date of current version 18 February 2025. This work was supported in part by the Delaware Space Grant College and Fellowship Program under NASA Grant 80NSSC20M0045, in part by the National Aeronautics and Space Administration under Grant NASA-80NSSC20M0220, and in part by the National Science Foundation under Grant NSF-IIS-484 2123264. *(Corresponding authors: Lingsheng Meng; Xiao-Hai Yan.)*

Deanna Edwing and Xiao-Hai Yan are with the School of Marine Science and Policy, University of Delaware, Newark, DE 19716 USA (e-mail: xiaohai@udel.edu).

Lingsheng Meng is with the School of Marine Science and Policy, University of Delaware, Newark, DE 19716 USA, and also with the College of Environment and Ecology, Xiamen University, Xiamen 361005, China (e-mail: lsmeng@udel.edu).

Suna Lv is with the College of Ocean and Earth Science, Xiamen University, Xiamen 361005, China.

Digital Object Identifier 10.1109/JSTARS.2025.3530255

of the coastline where water levels vary over time [12], [13]. Although employed over the global landscape [14], [15], [16], the vast majority of CNNs applied to case studies in the United States have targeted regions in the Southeast (SE) US where active annual hurricane seasons provide ample opportunity for network development and application. Furthermore, analysis typically targets only the most considerable flooding events, such as those frequently associated with the passing of major hurricanes. Recent examples are Hurricanes Harvey [17] and Florence [18], which primarily impacted states along the gulf and SE US coasts. Thus, states like Delaware and New Jersey, which have been historically sheltered from frequent extreme storm events, are largely ignored despite experiencing frequent enough flooding to pose issues to coastal communities.

Delaware Bay separates Delaware's peninsula from mainland New Jersey. It is susceptible to both river flooding from heavy rainfall and coastal flooding from cyclones via associated storm surge. Traditionally, surge is the focal point of flooding forecasts as it contributes most to storm-related deaths. Both extratropical and tropical cyclones produce storm surge, but tropical cyclone surge is more extensive in this region as they account for upwards of 45% of the top 10 and approximately 20% of the top 50 storm surge events in the Delaware and Chesapeake Bays [19]. Fortunately, tropical cyclone season is restricted to late summer and early fall in the northeast. Nor-easters, however, are a year-round occurrence. Unfortunately, as mean storm precipitation increases under climate change [20], surge may no longer solely dominate flooding concerns. Instead, the region is expected to become more susceptible to compound flooding events [6], [21], which result from the nonlinear interactions between storm surge, heavy precipitation induced river flooding, and astronomical tides [22], [23]. Coastal flooding and inundation in this region are therefore the net effect of numerous complex hydrodynamics which could serve to increase the frequency and intensity of coastal flooding [24].

Moreover, faster than average relative sea level rise rates [25] combined with high land subsidence [26], [27], [28] and increases in tidal range along northeastern US coastlines are increasing the frequency of nuisance flooding events [29] which occur during high tides in the absence of storm activity. The water level height during such events is based on mean higher high water (MHHW), land considered normally dry, and therefore serves as the point at which inundation typically occurs [4]. Not dependent on storm conditions, nuisance flooding can occur year-round; however, inundation occurs on a smaller scale in predictable coastal locations and will recede with the tide. Coastal storm events, however, have the potential to cause wider-scale flooding along the coast, as well as inundate inland regions if precipitation conditions are heavy enough. Therefore, the focus of this article is on floodwaters resulting from coastal storm activity instead of high-water levels resulting from higher-than-average tides.

The main challenge becomes, however, distinguishing between storm and tidal inundation. Studies typically use a prestorm and poststorm comparison for flood identification [18], [30], [31]; but this does not account for daily tidal variation, meaning flood water could be overestimated as flooding could be the result of both storm and astronomical tidal contributions. Flood detection is further complicated in this region as most of the bays, tributaries, and marsh wetlands surrounding Delaware Bay are hydrologically and tidally connected [32]. Therefore, distinguishing between flood waters, tidal inundation, and permanent water bodies is challenging. This study therefore develops an improved approach to isolating storm-induced floodwaters in complex coastal regions through the removal of permanent water bodies and tidal influence. Additionally, an exploration into how tidal water levels (WLs) and storm events individually and synonymously contribute to coastal flooding around Delaware Bay will provide a more comprehensive understanding of flood-vulnerable regions. This information will be useful for coastal residents, local government agencies, and managers alike.

This article uses Sentinel-1 SAR imagery in conjunction with a recently improved deep learning segmentation model by Lv et al. [33] to create multiyear flood maps of the Delaware Bay region from 2017-2021. Moreover, we design a new methodology that utilizes a series of products that help to identify coastal storm flooding and improve estimates through the removal of permanent water bodies and tidally inundated regions. Therefore, this article proposes a new approach to coastal flood identification through product development rather than the development or improvement of previous flood models. The impact of flooding on land use is also explored and summarized bay-wide and per event. The rest of this article is as follows: Section II provides the methodology for network training and data used for floodwater extraction, Section III reports model performance and floodwater analysis, and Section IV is a discussion on the impact of tides and factors contributing to the top three largest flooding events observed during the study period. Section V concludes this article.

II. Data and Study Region

A. Study Region

Delaware Bay (see Fig. 1) is characterized as a semi-enclosed estuarine environment created by the mixing of freshwater from the Delaware River and saltwater from the Atlantic Ocean. The bay is funnel shaped, approximately 45 km at its widest point [34], with an outlet to the Atlantic constrained by a narrow 17.5 km aperture between Cape Henlopen and Cape May [35]. The bay averages 7 m depth; however, deep scour in the middle lower part of the bay extends depths to deeper than 28 m [36]. The bay is bordered by the states of Delaware (coastal counties: Sussex, Kent, and New Castle) and New Jersey (coastal counties: Cape May, Cumberland, and Salem).

Delaware Bay is tidally influenced, with WLs fluctuating based on environmental factors, including coastline geometry, bottom friction and dissipation effects [37], as well as prevailing winds and ocean currents [24]. Converging coastlines in the north, towards the headwaters of Delaware Bay, amplify the tidal range to over 2 m compared to more modest levels (< 1.5 m) near the mouth [24], [38]. Mean tidal range is approximately 1.5 m [39]. Storm surge is similarly impacted, with the additional influence of storm-specific characteristics like size, direction of

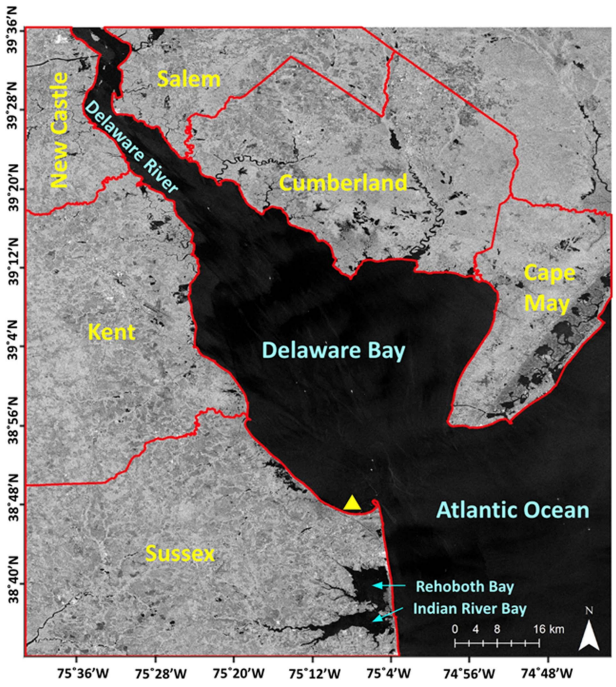

Fig. 1. Delaware Bay study area with Delaware counties (Sussex, Kent, New Castle) and New Jersey counties (Cape May, Cumberland, Salem) delineated in red and NOAA Lewes, DE tides and current buoy denoted by the yellow triangle. Major water bodies are noted in light blue and include the Delaware Bay and Delaware River, Atlantic Ocean, and the smaller Rehoboth and Indian River Bays.

travel, atmospheric pressure, storm duration, as well as wind speed and direction relative to the coastline [40]. Coastal flooding and inundation in this region are therefore the net effect of numerous complex hydrodynamics [24]. Therefore, flooding may impact the Bay's six coastal counties differently as different processes and mechanisms combine to amplify inundation in regions closer to the Bay mouth versus those closer to the Delaware River.

Except Cape May, agriculture is the dominant land cover over the entire region. However, the Delaware Bay shoreline is comprised of sandy beach, salt marsh, and developed lands [41], although studies have shown that salt marshes are declining due to a combination of factors including a rise in sea level [42] and agricultural/urbanization pressures [43]. The bay is fed by numerous smaller streams and rivers originating in both Delaware (i.e., Christina and Broadkill Rivers) and New Jersey (i.e., Salem and Maurice Rivers), and is home to many canals near the southern portion of both states (i.e., Lewes and Rehoboth Canals in Delaware, and Cape May Canal in New Jersey). Currents within the bay are dominated by the semi-diurnal tidal cycle and are oriented northwest-southeast along the primary axis of the bay [44].

B. SAR Imagery and Pre-Processing

The Sentinel-1 constellation comprises two polar-orbiting satellites launched in 2014 (Sentinel-1A) and 2016 (Sentinel-1B), which perform C-band SAR imaging. They can image in four exclusive modes with a minimum revisit time of 6 days, maximum spatial resolution of 5 m, and coverage up to 400 km. Sentinel-1 data is free and publicly available for download, and its high spatial resolution and good image quality make it practical for use in flood detection.

To analyze Delaware Bay coastal inundation, Sentinel-1 SAR imagery is downloaded between the years 2017 and 2021. Image availability is inconsistent and sparse prior to this period. Sentinel imagery of the study region is available approximately every 12 days, resulting in a dataset containing 136 images. All imagery used in this study are Level-1 interferometric wide swath ground range detected (GRD) products with VV-polarization and 10 $\times$ 10 m resolution. These images serve as inputs to the neural network from which water maps are created and subsequently used to make observations about tidal inundation and coastal flooding around Delaware Bay.

Image preprocessing steps include: radiometric calibration, geometric terrain correction, a 7 $\times$ 7 Refined Lee filter to reduce speckle, and subset generation so images match geographically. Additionally, all images undergo local brightness enhancements to increase the contrast of the overall image. Finally, image files are batch converted to PNG format.

TABLE I
SIX SENTINEL-1 GRD IMAGES USED TO CREATE THE MODEL TRAINING DATASET

Image ID	Usage	Imagery Date	Notes
Scene 1	Non-Flooding	06/10/2017	Non-storm
Scene 2	Non-Flooding	02/05/2018	Non-storm
Scene 3	Flooding	08/05/2020	Hurricane Isaias
Scene 4	Flooding	12/27/2020	Storm
Scene 5	Flooding	09/05/2021	Hurricane Ida
Scene 6	Flooding	04/09/2022	Storm

Note: Four images are taken just after the passing of a storm event, two of which include hurricanes. This training dataset therefore includes a variety of weather conditions experienced around Delaware Bay.

C. Training Dataset Generation

To generate a training dataset for the deep learning model, we select six Sentinel-1 GRD images captured between the years 2017 and 2022. Four out of six images are captured after the passing of storm activity with reported flooding, two of which include hurricane events (see Table I). The training dataset, therefore, includes a variety of weather conditions experienced around Delaware Bay, including 1) standard/everyday, 2) thunderstorm, and 3) storm/hurricane.

To generate the ground truth labels associated with training images, we implement LabelMe software [45], an online annotation tool used to manually define water bodies. Labels are batch converted from json to png format, divided into 256 x 256 subimages, and augmented with a 100-pixel vertical shift. The

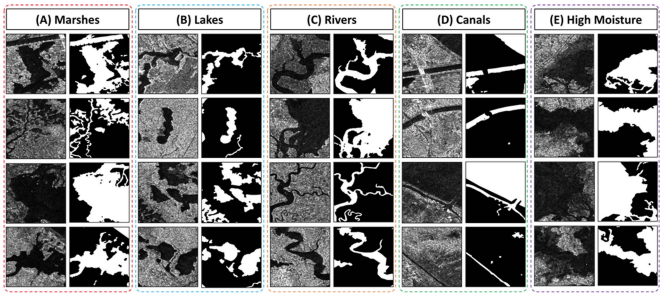

Fig. 2. Samples of water bodies contained within the training dataset for Modified DeepLabv3+ including water in (a) marshes, (b) lakes, (c) rivers, (d) canals, and (e) high moisture environments. SAR imagery of the water body is on the left and the corresponding ground-truth label on the right.

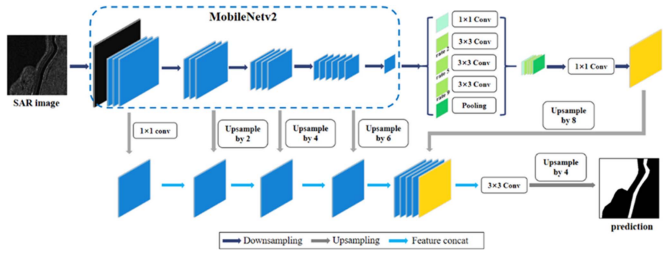

Fig. 3. Architecture of the modified DeepLabv3+ neural network from Lv et al. [33].

complete dataset consists of 21 980 subimagery pairs, which are randomly allocated to 70% training (15 386 pairs), 15% validation (3297 pairs), and 15% testing (3297 pairs). Fig. 2 provides a few examples of the pairs contained within the training dataset.

D. Ancillary Geospatial and Oceanographic Data

Analysis of coastal flooding is based on flood maps created using outputs from the trained model. This analysis is aided using ancillary oceanographic and geospatial datasets including tides and water level data, and land cover classification products. Tidal stage and WL conditions with respect to MLLW are acquired at 6 p.m. EST for each image via the Lewes, DE NOAA Tides and Current Buoy. Datums specific to the Lewes buoy are provided by NOAA and used to define high and low tide periods. Between 2017 and 2021, WLs in imagery fluctuated between –0.075 and 2.146 m extrema with low tide generally congruent with WLs below 0.10 m and high tide congruent with WLs higher than 1.0 m. MHHW is defined as approximately 1.50 m at the mouth of the Bay, increasing to 1.90 m toward the headwaters as the Bay becomes topographically confined.

To determine which images corresponded to coastal storm events, image acquisition dates were cross-referenced with the Delaware coastal storm dataset (DCSD), which records coastal storm events with strong low-pressure systems and therefore the potential to impact Delaware. These storm systems were further cross-referenced with precipitation events using the National Weather Services' advanced hydrological prediction service precipitation. Most storms corresponded to multiday precipitation events with a few exhibiting precipitation a couple days prior to the arrival of the strong low-pressure system off the Delaware Bay coastline. Therefore, storm imagery is defined as having a Sentinel-1 image equivalent to or the day following a recorded DCSD event in addition to precipitation within at least 3 days of the recorded storm event. This provides 23 storm events in addition to the three 2020–2021 events used in training for a total of 26 storm events.

All land cover information used in this study is provided by the 2019 National Land Cover Database (NLCD) product [46] which classifies land surfaces into 16 classes at 30 m spatial resolution [47]. However, for the purposes of this study, these classes were regrouped into cropland, wetland (also referenced as marsh), urban, and other. This product was used to determine areas of tidal influence, as well as which land cover classes were most impacted by flooding.

III. Methodology

A. Neural Network Design

Modified DeepLabv3+ is a network modified by Lv et al. [33] as an improvement to DeepLabv3+, an encoder–decoder semantic segmentation network released by Google in 2018 [48]. The improvements made by Lv et al. [33] in the Modified DeepLabv3+ (see Fig. 3) network include the following.

1) The selection of MobileNetv2, a lightweight network, as the network backbone to improve water detection efficiency.
2) The introduction of small, jagged arrangement atrous convolutions to capture small-scale water bodies and improve pixel utilization.
3) Increasing the number of upsampling layers to refine water body boundaries.

The network operates in such a way that the encoder module uses MobileNetv2 to create a feature map from which multiscale features are extracted through Atrous Spatial Pyramid Pooling. The decoder module then uses a skip connection structure to construct four upsampling layers which accumulate information from three branches within its structure [33]. The first is from low-level features obtained by a 1 x 1 convolution of the MobileNetv2 network to reduce their dimensionality. The second is from the output of the newly added upsampling layers, which undergo bilinear interpolation upsampling to acquire the same resolution as lower-level features. The final branch is a feature map created by fusion of the ASPP output after a 1 x 1 convolution and eight iterations of bilinear interpolation upsampling [33]. The final network prediction (hereafter referred to as a water map) is produced through the fusion of information from these three branches, followed by 3 x 3 convolution and four iterations of bilinear interpolation upsampling [33].

Model outputs are binary maps with water detections marked as 1 and nonwater as 0. Training runs were performed with training epochs set to 300, batch size to 32, and initial learning rate to 0.001 with a ploy learning strategy.

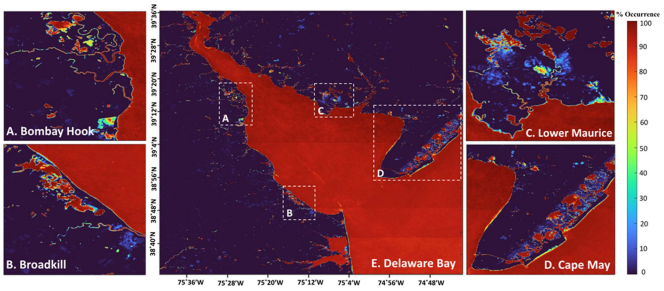

Fig. 4. Water occurrence of (e) Delaware bay highlighting (a) Bombay Hook (Kent County, DE), (b) Broadkill (Sussex County, DE), (c) Lower Maurice (Cumberland County, NJ), and (d) Cape May (Cape May County, NJ) areas to elucidate localized patterns. Water above 80% occurrence is defined as permanent water.

B. Removing Permanent Water Bodies

Using the trained model on 136 Sentinel-1 SAR images reveals general water presence around Delaware Bay from 2017–2021 in a single product known as water occurrence (see Fig. 4). Each Sentinel-1 image results in the creation of a binary water map (model output) and the per-pixel summation of water detections over all model outputs creates water presence frequency around Delaware Bay. These totals are then divided by the number of water maps and multiplied by 100 to create an occurrence percentage. A high occurrence value indicates that the Modified DeepLabv3+ model identified a pixel as water more frequently, whereas lower occurrences indicate that water was not detected as frequently in those areas. Fig. 4(a)–(d) provides close-ups of four locations that depict a comprehensive view of conditions ranging from high occurrence in dark orange/red t anomalously inundated areas (low occurrence) in the light blues. Therefore, this product creates a distribution of water presence which allows water to be separated into useful classes for eventual flood water isolation. Such classes include the presence of permanent water and tidal inundation which need to be removed prior to flood water analysis.

The ability to differentiate higher water occurrences allows us to define a threshold for permanent water bodies as those with occurrences greater than 80%, corresponding to the dark orange to red colors in Fig. 4. This threshold was determined based on visual assessment of the occurrence layer against known permanent water bodies like the Delaware Bay and many of the smaller bays, main feeder rivers, and smaller inland lakes and ponds both naturally and artificially occurring in the region. Similar methods and thresholds have been used in other studies like Olthof and Rainville [49].

Permanent water bodies serve as a baseline for the mean state of Delaware Bay water; in other words, their locations indicate the expectancy of water presence on any given day. All other captured water is nonpermanent and denoted in blue to light orange colors, representing areas where water occurs more intermittently (green) to less frequently (blue). These lower occurrence regions most likely correspond to potential flooding since storm-related imagery are the minority in the dataset and not all storm events result in flood activity. However, the flooding signal is likely intermingled with tidal influence as the relatively flat topography and coastal location can result in extensive tidal inundation. Therefore, lower occurrence regions need to be further explored to isolate storm-related flood waters.

Altogether, this product reveals water occurrence variability in the Delaware Bay region, providing one method to segregate permanent water from anonymously inundated regions which could potentially be the result of daily tidal cycles or storm activity. Permanent water bodies identified here are exported to serve as a mask in future analysis.

C. Removing Tidal Inundation

Delaware Bay experiences two daily tidal cycles, meaning WLs fluctuate between their extrema as the tide ebbs and floods, reaching peak levels during high and low tidal periods. These rises in WLs result in temporary inundation of primarily marshes and contribute to the lower occurrence water present in Fig. 4. The low-lying and relatively minimal topographic relief of Delaware and New Jersey means that the horizontal extent of daily cycles could result in significant inundation unrelated to storm activity. Therefore, to isolate water present only because of coastal storms and not the natural variability of daily tidal cycles, the influence of tidal inundation needs to be removed. This natural variability is accounted for in a novel product known as maximum tidal extent.

Maximum tidal extent is determined using composites of imagery acquired during nonstorm periods corresponding to WLs above low tide (WLs $>$ 0.10 m). Recall that tidal information is provided by the Lewes, DE tidal buoy. Maximum tidal extent is taken to be water identified by the model in regions classified as wetlands by the NLCD, in addition to water along shoreline regions of Delaware Bay permanent water bodies and their main tributaries. Furthermore, inspection was performed to limit any additional water outside marsh regions which may have been included during product creation. It should be noted that in the creation of the maximum tidal extent product, three storm images were misidentified as nonstorm and are therefore included in the product. The inclusion of these storms could mean that the maximum tidal extent includes floodwater if the storms produced coastal flooding near tidally influenced regions. By recreating the product without storm events included, the additional per-county contribution of these storms to the product was determined to be: 0.0803 km^2 in Cape May, 0.0529 km^2 in Cumberland, 0.0358 km^2 in Salem, 0.1005 km^2 in Sussex, 0.0747 km^2 in Kent, and 0.0103 km^2 in New Castle. Therefore, flood estimates could potentially be underestimated by these amounts per-county.

Based on the created product, tidal inundation extent is largest in regions near the Bay mouth and decreases in areas nearest the Delaware River. Areas of extensive tidal inundation are patchy [see Fig. 5(a)–(d)] but highlight regions like Cape May where tides can potentially inundate almost the entire coastal marsh area depending on WL height [see Fig. 5(d)]. In general, tidal inundation results in a slight widening of Delaware Bay [see Fig. 5(c)], as well as swelling of many rivers and inland water bodies [see Fig. 5(b)] and temporary creation of small ponds in regions immediately adjacent to the Bay [see Fig. 5(a)].

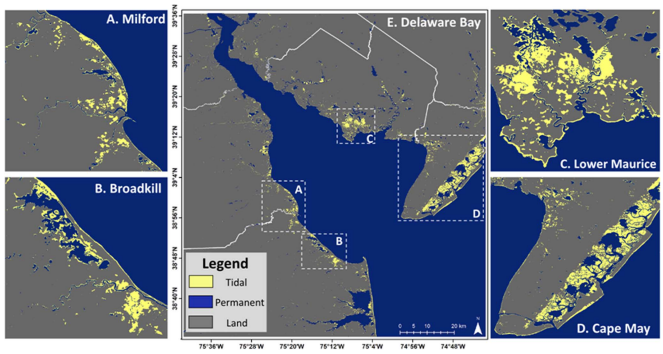

Fig. 5. Maximum tidal extent shows tidally influenced regions around Delaware Bay (e), highlighting four regions which experience significant tidal influence including (a) Milford (Kent County, DE), (b) Broadkill (Sussex County, DE), (c) Lower Maurice (Cumberland County, NJ), and (d) Cape May (Cape May County, NJ). Solid white lines delineate county boundaries.

TABLE II
QUANTIFICATION OF MAXIMUM TIDAL EXTENT AROUND DELAWARE BAY'S SIX COASTAL COUNTIES

State	County	County Area (km^2)	Coastline Length (km)	Marsh Area (km^2)	Tidal Inundation (km^2)
New Jersey	Cape May	837.5982	71	412.3263	89.364
	Cumberland	1683.6743	67	577.1952	43.2154
	Salem	708.5447	40	243.4195	8.575
Delaware	Sussex	2479.5992	61	529.7801	38.8962
	Kent	1707.1477	57	538.6121	26.4539
	New Castle	477.3475	34	142.9788	5.7597

Quantifying maximum tidal extent per county reveals that Cape May and Cumberland counties experience the most tidal inundation, followed by Sussex and Kent, with Salem and New Castle counties experiencing the smallest tidal inundation (see Table II). These values also appear to correlate with coastline length, however other factors such as topographic relief can also influence tidal inundation location. Regardless, the patchy distribution of extensive tidal inundation emphasizes the importance of removing this water from flood analysis, especially in southern counties where tides can impact over 89 km^2. Removal of tidal water ensures that flood identification is limited to areas with minimal tidal influence; therefore, the maximum tidal extent product serves to improve flood estimates as values reflect storm contributions rather than daily tidal inundation.

Although these results are specific to Delaware Bay, overall trends can be extrapolated to similar coastal bay systems, such as the Chesapeake, which experiences daily water fluctuations. Therefore, bays located on the flat coastal plain can expect patches of extensive tidal inundation in regions closer to the mouth that decrease heading upstream. Longer coastlines with larger marsh systems also correlate with larger tidal extents. Under future climate change conditions, the use of tidal masks will become increasingly important as other factors such as rising sea levels will likely result in increasingly larger tidal inundation extents. So, to ensure flood estimates reflect only the influence of the storm events rather than daily tidal activity, maximum tidal extent is removed prior to analysis.

D. Flood Water Identification

To analyze Delaware Bay coastal flooding, flood waters are extracted from 26 images that meet storm definition criteria. To isolate storm-induced flood waters, nonstorm related waters are systematically masked and removed using the following information.

1) A pre–post storm difference to remove water that is similar between the two dates, where the prestorm map is the closest nonstorm date prior to the storm event and the poststorm map is the storm event identified using the DCSD.
2) Water mask generated from
   a) permanent water above 80% occurrence;
   b) maximum tidal extent;
   c) water corresponding to the NLCD "open water" class. It is extracted from nonstorm imagery to provide an additional check to the permanent water classification.

IV. RESULTS

A. Model Performance

Model performance is quantitatively analyzed using five evaluation indicators:

$$\text{Accuracy} = \frac{\text{TP} + \text{TN}}{\text{TP} + \text{TN} + \text{FP} + \text{FN}} \tag{1}$$

$$\text{Recall} = \frac{\text{TP}}{\text{TP} + \text{FN}} \tag{2}$$

$$\text{Precision} = \frac{\text{TP}}{\text{TP} + \text{FP}} \tag{3}$$

$$\text{Dice Coefficient} = \frac{2 * \text{Precision} * \text{Recall}}{\text{Precision} + \text{Recall}} \tag{4}$$

$$\text{Intersection over Union (IoU)} = \frac{\text{TP}}{\text{TP} + \text{FP} + \text{FN}} \tag{5}$$

where True Positives (TP) are the number of water pixels correctly identified as water, False Positives (FP) are the number of nonwater pixels incorrectly identified as water, True Negatives (TN) are the number of nonwater pixels correctly identified as nonwater, and False Negatives (FN) are the number of water pixels incorrectly identified as nonwater pixels.

Accuracy (1) is defined as the proportion of pixels correctly classified as water and nonwater out of the total number of pixels within the image. Recall (2) is the proportion of pixels correctly classified as water to the total number of water pixels present within the image, and precision (3) is the proportion of pixels correctly classified as water pixels to all pixels correctly or incorrectly identified as water. The Dice coefficient (4) refers to the harmonic average of recall and precision. Finally, Intersection over Union (IoU; 5) describes how well the *(x,y)* coordinates of the predicted water feature class from the network prediction match the *(x,y)* coordinates (i.e., true location) of the ground-truth water bodies identified in each image label. Mean IoU (mIoU) results from averaging the summation of these intersection ratios.

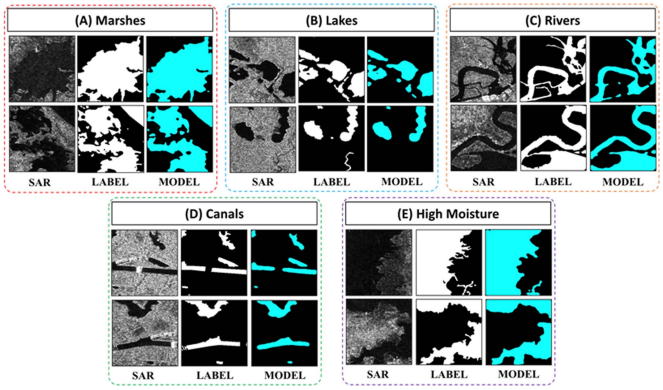

Fig. 6. Visualization of water segmentation results from Modified DeepLabv3+ for water in (a) marshes, (b) lakes, (c) rivers, (d) canals, and (e) high moisture environments.

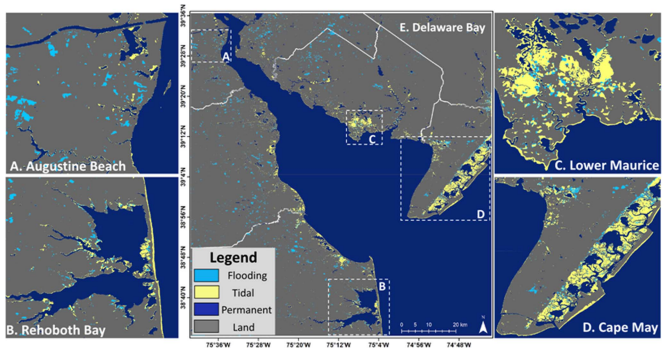

Fig. 7. Spatial map of Delaware Bay (e) flooding resulting from storm events between 2017 and 2021 at (a) Augustine Beach (New Castle County) and (b) Rehoboth Bay (Sussex County) in Delaware, and (c) Lower Maurice (Cumberland) and (d) Cape May (Cape May County) in New Jersey. Solid white lines delineate county boundaries.

Overall, model performance results indicate that the model can accurately and consistently segment water bodies in SAR imagery. The model achieved an accuracy of 0.985, indicating that the model can classify nearly all labels correctly. A precision of 0.987 and a recall of 0.967 indicate that the model does not often misclassify true positive water pixels, as the high metric scores mean there is a low probability of the model producing a false negative or false positive. Therefore, the model can distinguish well between water and nonwater pixels. A dice coefficient of 0.977 indicates the model's high capability to both identify water pixels (recall) and be accurate in this water identification (precision). Finally, an mIoU score of 0.966 means the model's water predictions highly correlate with the positioning of the ground truth water, meaning the model can both accurately quantify and spatially correlate its water predictions to the input image.

Fig. 6 provides a visual representation of Modified DeepLabv3+ model performance, comparing ground truth labels to model predictions of various water body types around Delaware Bay including water in marsh areas [see Fig. 6(a)], natural and artificial lakes [see Fig. 6(b)], rivers [see Fig. 6(c)], canals [see Fig. 6(d)], and examples of more complicated terrain where high moisture regions mimic water backscatter signals [see Fig. 6(e)]. In general, segmentation results are consistent with ground truth labels, having a low false alarm rate. Extracted water bodies also have clear and complete boundaries. Furthermore, the model can distinguish between standing water and high moisture environments such as the tidal marsh, where soil moisture and wet vegetation can result in a backscatter signal similar to that of water [see Fig. 6(e)]. Overall, the model's ability to accurately extract water bodies with clear and complete boundaries supports the conclusion of a successful training performance and indicates that the Modified DeepLabv3+ is ready for flood water application in the Delaware Bay region.

B. Delaware Bay Coastal Flooding

Resulting flood maps from the 26 storms are superimposed to depict locations where storm-related flooding occurred at least once in that location around Delaware Bay (see Fig. 7).

Between 2017 and 2021, a total of approximately 139.8 km^2 of flooding was detected around the Delaware Bay region, with Sussex and Kent counties contributing the most with 28.6% (39.9 km^2) and 21.0% (29.4 km^2), respectively. The remaining counties contributed the rest with Cape May providing 12.8% (17.9 km^2), Cumberland providing 18.0% (25.1 km^2), Salem providing 12.2% (17.1 km^2), and New Castle providing 7.4% (10.3 km^2). Spatially, flooding impacted both coastal and inland regions around Delaware and New Jersey. Coastline flooding was primarily concentrated around tidally influenced regions and caused additional swelling and overtopping of heavily tidally impacted water bodies [see Fig. 7(c)]. This is especially apparent in the Cape May region [see Fig. 7(d)] where almost the entirety of the eastern side has the potential to become inundated. Northern counties such as New Castle and Salem appear to be dominated by inland flooding events as the impact of tides is less apparent in these regions [see Fig. 7(a)]; however, dense clusters of flooding are still found along river edges, possibly indicating the result of river overwash into these locations.

Quantification of individual storm events revealed that there was a wide distribution of total flooding; however, most storm events resulted in less than 5 km^2 over the entirety of the study region (see Fig. 8). Distributed over the six coastal counties, most events result in less than 2 km^2 of flooding per county, with Sussex and Kent counties in Delaware and Cumberland County in New Jersey experiencing the largest variability (see Fig. 8). However, outliers above the box and whiskers represent storm events which resulted in abnormally large flooding area. Three events were responsible for between 19.2 and 55.8 km^2 of total flooding, and represent the outliers present above the county flooding breakdown boxes. Total flooding for the largest event was excluded in Fig. 8 for display purposes but accounted for 10 km^2 of flooding in four of six counties. This means that a lot of the flooding in Fig. 7 was likely the result of a few intense events.

C. Land Cover Impacts of Detected Flooding

It is apparent that Delaware Bay is a hydrodynamically complex environment. Extensive tidal inundation was observed

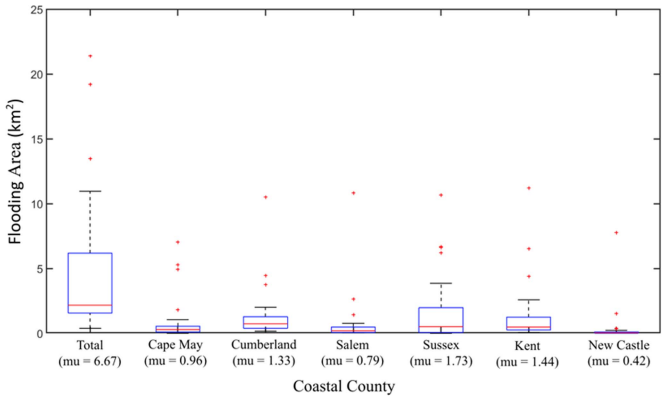

Fig. 8. Distribution of individual storm event contributions to flooding reported per county between 2017 and 2021. A value of 55.8 km^2 was excluded for display purposes but exists as an outlier present in the Total category.

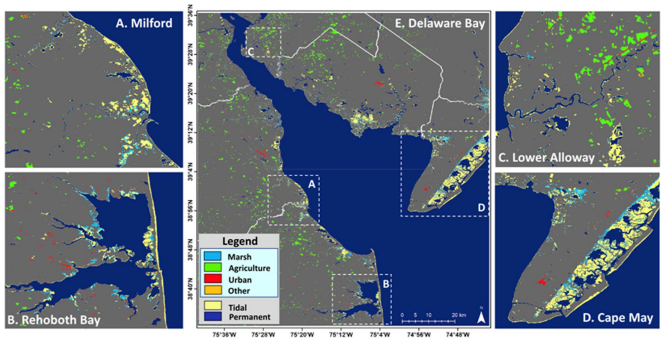

Fig. 9. Spatial map of (e) Delaware Bay flood waters classified based on their land cover impacts, with close-up examples provided for (a) Milford (Kent County, DE), (b) Rehoboth Bay (Sussex County, DE), (c) Lower Alloway (Salem County, NJ), and (d) Cape May (Cape May County, NJ). Flood water classes are provided in the blue box in the legend with permanent water in dark blue and tidal waters in light yellow. Solid white lines delineate county boundaries.

when WLs were suitably high, with inundation further exacerbated by flood conditions; or flooding occurred away from the coastline in inland regions. To determine the resulting land cover impact, flooding locations were compared to the 2019 iteration of the NLCD. This comparison allowed flood water to be classified based on its corresponding land cover impact.

Spatial analysis revealed that coastal flooding adjacent to the bay or main tributaries was absorbed by tidal marsh, while inland flooding primarily impacted agricultural areas near smaller feeder rivers (see Fig. 9). Urban flooding was observed but extremely localized. Comparison to World Street Maps in ArcMap revealed impacts were primarily to roads and neighborhoods adjacent to large rivers and inland bays, as well as to airports which are denoted as the three large red areas in Cape May, Cumberland, and Kent counties (see Fig. 9).

Quantifying this spatially, the land cover that was predominantly flooded around Delaware Bay was agriculture, which impacted approximately 97.0 km^2 (69.4%) followed by marsh at 28.4 km^2 (20.3%). Their combined impact accounted for 89.7% of all areal flooding in the Delaware Bay region, with urban (8.9 km^2) and other (5.4 km^2) accounting for the remaining

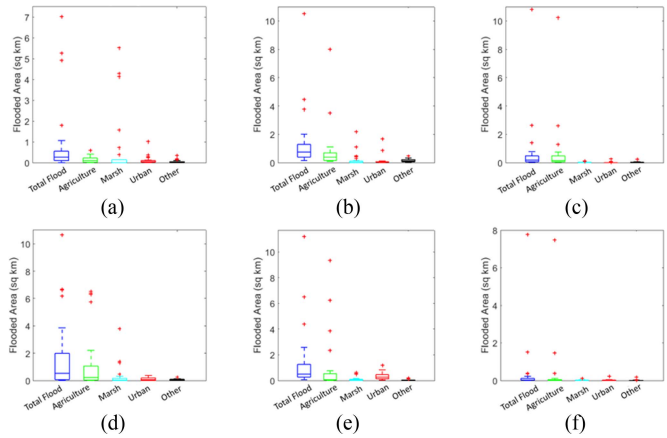

Fig. 10. Coastal county breakdown of flood water land cover impacts reported for 26 storm events with land cover summaries for (a) Cape May, (b) Cumberland, (c) Salem counties in NJ, and (d) Sussex, (e) Kent, (f) New Castle counties in Delaware.

10.3% . The dominance of agricultural flooding is most likely due to the Delaware Bay region being agriculturally dense compared to other land cover classes. Analysis therefore highlights the potential negative impacts flooding can have on agricultural fields in this region. This trend holds true for all counties except Cape May, where the dominant flooded land cover was marsh (77.2%) followed by urban areas (10.0%). This is most likely due to Cape May experiencing more flooding along coastline regions rather than more inland locations. Additionally, Cape May's natural land cover is not as agricultural dense compared to other counties; instead, natural land cover is dominated by marsh and urban regions thereby explaining their larger flood impacts.

These trends are further reinforced by an event-specific county breakdown, where land cover impacts were summarized for each storm event (see Fig. 10). Like the spatial distribution, flooding primarily impacted agriculture. However, Cape May was still considered to be marsh flood dominated due to the presence of numerous outliers within the marsh estimates that were not present in the agricultural estimates (see Fig. 10). This indicated that the large spatial extent of marsh flooding in Cape May [seen in Fig. 9(d)] is the result of a couple larger events rather than the composite of multiple smaller scale flooding events.

Overall, the relatively small per-storm land cover flood contributions highlight that most of the spatial flooding observed in Fig. 9 is likely the result of a few strong storm events that resulted in extensive areal flooding, producing the outliers present within each county land cover summary (red crosses in Fig. 10).

V. Discussion

Results of the proposed methodology yielded storm-flood estimates for Delaware Bay, providing an opportunity to understand the scale of regional flooding to coastal storm activity and their environmental impacts. It was shown that the Delaware Bay region is vulnerable to coastal storms with agricultural and marsh regions facing the largest impacts of flooding. This engenders questions about the necessary storm conditions and mechanisms

behind large-scale flood events. Section V-A explores this by using case study events to characterize general flooding trends by correlating flood-response to associated storm attributes. The discussion ends with a review of the products used to improve stormwater identification in Sections V-B and C.

A. Case Study Events

Results in Section III-D revealed that three storm events produced the largest flooding. These three events are further examined to determine their individual impacts and the potential mechanisms behind their large flood contributions. These mechanisms are then used to characterize regional flood response to future storm events exhibiting similar attributes.

1) Case Study Number 1: October 2019: A slow-moving 1004 mb low-pressure system moved off the coast of Delaware Bay between 8 and 12 October 2019 with Sentinel-1 imagery of this event available on the evening of 10 October 2019. The system produced a three-day precipitation event which averaged between 0.25 and 12.7 mm per day over the region. Prior to this event, several isolated storms produced scattered rain events primarily over New Castle, Salem, and northern parts of Kent and Cumberland counties. Between October 8 and 12, wind direction remained constant from the Northeast with wind speeds ranging primarily from 8–12 m/s with short periods of winds at higher speeds between 12 and 14 m/s. At the time of imagery acquisition, water level was 2.146 m above MLLW; moreover, the system produced several consecutive high tide cycles from 9 to 10 October which produced minor to moderate coastal flooding events according to the National Weather Service (MWS).

These conditions combined to create the largest flood event in this dataset, covering a combined 55.8 km^2 over the Bay's six coastal counties. Comparison to the NLCD revealed significant impacts to agricultural regions (41.7 km^2), with large marsh flooding occurring in the southernmost counties of Cape May (4.1 km^2) and Sussex (3.8 km^2) [see Fig. 11(h)]. Though marsh flooding was more prevalent along DE's bay coastline [see Fig. 11(e) and (f)]. Urban impacts were mainly on airports and roads. Parts of a military airport in Cumberland County, Kent County's airport, and a small private airport in Cape May experienced patchy flooding, most likely due to their open, flat topography resulting in water accumulation from the multiday precipitation event. Localized flooding was observed in neighborhoods adjacent to large tidally influenced water bodies such as Rehoboth Bay in Sussex County, DE and is most likely a consequence of the high water-level conditions at the time of imagery acquisition.

The large size of this event was likely a response to a combination of high water-levels, a multiday precipitation event with previous ground moisture from scattered showers, as well as consistent wind direction that exacerbated increased WLs. Within the bay, high water levels combined with northeasterly winds to push water towards the Delaware side of the Bay, most likely contributing to the more extensive marsh flooding in Sussex County (3.8 km^2) compared to those along the New Jersey side of Delaware Bay such as Cumberland (0.4 km^2). This

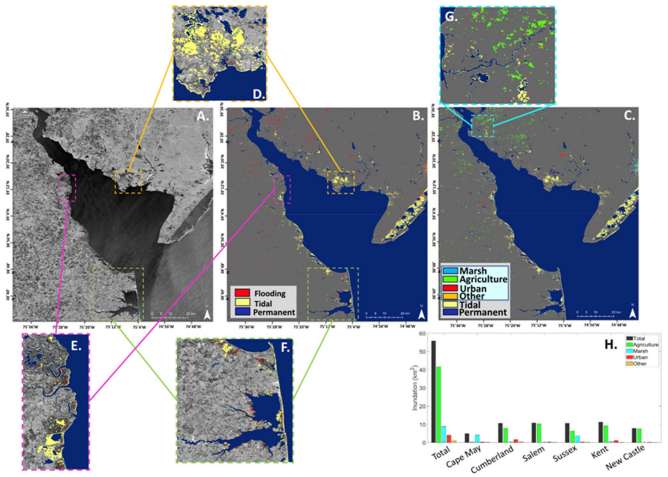

Fig. 11. Flood maps for the October 10, 2019 flood event. (a) Storm event SAR image. (b) Flood map with flood water denoted in red. (c) Flood water classification map with flood water classes provided in the blue box in the legend. (d)–(f) Subsets of flooding from B superimposed on A to highlight the impact of wind on marsh flooding differences between New Jersey (d) and Delaware (e)–(f) coastlines. (g) Subset of panel C showing urban road and agricultural flooding. (h) Per-county summary of classified flood waters.

also explains the marsh flooding experienced along the Atlantic-facing coastlines of Cape May where wind helped push water into these regions. Furthermore, successive high tides which were large enough to be classified as flooding by the NWS, likely contributed to the urban and agricultural flooding experienced in regions close to Delaware Bay or its tributaries. Precipitation also contributed to the inland agricultural and airport flooding observed during this event. It should be noted that image quality impacted the easternmost portions of Cape May and southern parts of Sussex County, primarily in the marsh regions. This means that this event was likely larger than current estimates, particularly the marsh flooding estimates, but was unable to be quantified based on model performance.

2) Case Study Number 2: April 2021: From 25–26 April 2021, a low-pressure system with an initial pressure of approximately 1006 mb at its center on the 25th and 996 mb on the 26th migrated off the coast of Delaware Bay; with Sentinel-1 imagery available the evening of 26 April. It resulted in a two-day precipitation event with most of the precipitation occurring on the 25th. Precipitation ranged between 6.4 and 38 mm on the 25th, before decreasing to 0.25–2.5 mm on the 26th which primarily impacted regions along the Delaware coastline and inland regions in New Castle County. Wind direction fluctuated between southerly and easterly directions at varying speeds generally ranging between 6 and 12 m/s. Although periods of higher speeds between 12 and 14 m/s were also observed. At the time of imagery acquisition on 26th April, water level was at 1.303 m above MLLW; however, the previous day saw one high tide cycle encroach on minor flooding status.

These conditions combined to produce a 21.4 km^2 flooding event [see Fig. 12(g)] with most of the flooding impacts to inland agricultural regions [20.5 km^2; Fig. 12(c)]. As there was little to

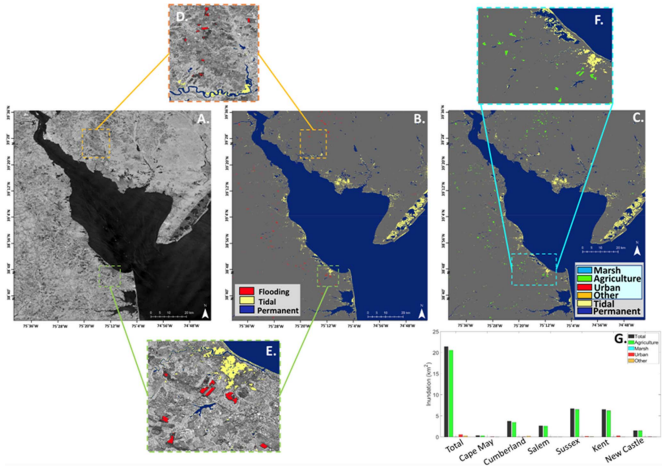

Fig. 12. Flood maps for the April 26, 2021 flood event. (a) Storm event SAR image. (b) Flood map with flood water denoted in red. (c) Flood water classification map with flood water classes provided in the blue box in the legend. (d), (e) Subsets of flooding from B superimposed on A to show agricultural flooding both inland (d) and closer to coastal marshes (e). (f) Subset of panel C showing inland and coastal agricultural flooding in Sussex County, DE. (g) Per-county summary of classified flood waters.

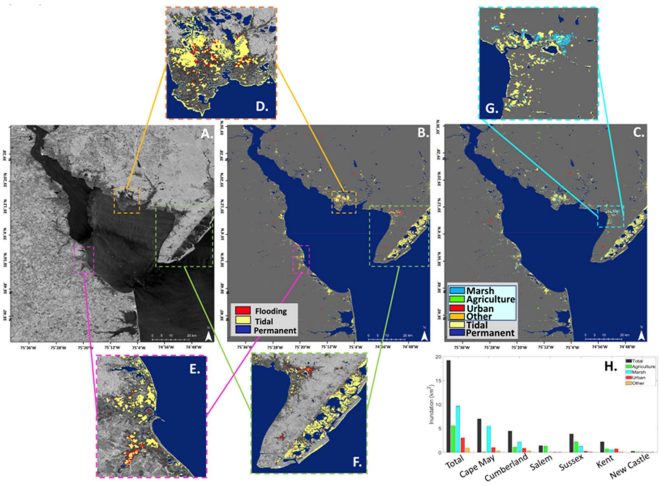

Fig. 13. Flood maps for the 11 July 2018 flood event. (a) Storm event SAR image. (b) Flood map with flood water denoted in red. (c) Flood water classification map with flood water classes provided in the blue box in the legend. (d)–(f) Subsets of flooding from B superimposed on A to highlight the impact of wind on coastal marsh flooding along New Jersey (d,f) and Delaware (e) coastlines, (g) Subset of panel C showing marsh flooding in Cape May, NJ which contributed the largest to marsh flooding for this event. (h) Per-county summary of classified flood waters.

no marsh flooding (0.01 km^2), this large event was most likely the result of intense precipitation on the 25th. This is supported by the locations of the agricultural flooding which is primarily concentrated along inland regions where agriculture fields are dense rather than along the coastline [see Fig. 12(d)]; although some flooded crops lie near coastal marsh and tidal regions [see Fig. 12(e)].

3) Case Study Number 3: July 2018: Hurricane Chris was a moderately strong tropical cyclone which impacted the east coast between 6 and 12 July 2018; with Sentinel-1 imagery of this event available the evening of 11 July. It had a central pressure of around 912 mb and moved slowly along the Mid-Atlantic coastline where it remained offshore for several days. An intense two-day rainfall event occurred several days before imagery acquisition on 6–7 July which produced upward of 51 mm per day primarily in southern Delaware and New Jersey. As Hurricane Chris remained farther offshore, sustained wind speeds on 10–11 July were relatively mild, typically around 3.0 m/s originating primarily from the SW though direction was highly variable during this time. At the time of imagery acquisition, water levels reached 1.77 m above MLLW and fell on the border of minor flooding according to NWS classification.

These conditions resulted in 19.2 km^2 of flooding around Delaware Bay [see Fig. 13(h)], with primary impacts to marsh (9.6 km^2) followed by agricultural regions (5.6 km^2). Urban impacts were observed for this event but were concentrated in Cape May, Cumberland, and Kent counties where the three major airports in this study region are located [see Fig. 13(c)]. Neighborhoods adjacent to larger inland water bodies such as Indian River Bay in Sussex County, DE showed small, localized patches of inundation which most likely were caused by high water level conditions at the time of imagery acquisition. Extensive marsh flooding is observed along both New Jersey [see Fig. 13(d) and (f)] and Delaware [see Fig. 13(e)] coastlines. This is most likely the result of the variable wind direction which pushed water toward both coastlines and up into the Bay itself. Agricultural flooding was likely the result of either tidal over wash from riverine/marsh regions if located near these areas or remnants from the precipitation from 6–7 July 2018. Overall, variable wind direction and high-water levels resulted in the third largest recorded flooding event with flood waters primarily impacting marshes surrounding the main Bay body. Remnants from a precipitation which occurred a couple days prior also contributed to the agricultural flooding observed during this event.

4) Delaware Bay Flooding Characterization: Case study analysis explored the impacts and potential conditions that contributed to the top three detected flooding events in the Delaware Bay region. The October 2019 flood event was likely produced from a multiday precipitation event combined with several consecutive high tides that reached minor/moderate flood level classification. This resulted in flooding primarily to agriculture and coastal marshes, with northeasterly winds contributing to larger marsh flooding along Delaware's coastline. The April 2021 event likely resulted from intense precipitation with impacts focused on inland agricultural regions. Finally, during the July 2018 event, variable wind direction combined with high water levels contributed to the extensive marsh flooding along both Delaware and New Jersey coastlines. Agricultural flooding during this event likely resulted from a combination of remanent water from a multiday precipitation event several days prior, as well as overwash from high water levels. Across all events, urban impacts were relatively minor but mostly impacted roads, airports, and coastal neighborhoods.

Based on these findings, general characterizations can be made about flooding in Delaware Bay. Overall, the largest flood events tend to occur during a convergence of high water-levels

and recent multiday precipitation events. Extensive coastal flooding occurs when WLs exceed MHHW levels and can be further exacerbated by multiple consecutive high tides reaching minor/moderate flooding stage. Large flood events also occur as the result of intense precipitation (i.e., April 2021). With most impacts concentrated on inland agricultural regions. However, agricultural flooding also occurs in coastal regions, indicating that agricultural flooding could result from either river overtopping into adjacent regions (i.e., October 2019) or from precipitation (i.e., April 2021). However, many other factors also contribute to agricultural water logging such as soil moisture, soil type, crop type and density. Therefore, further exploration is needed to explain inland flooding trends in Delaware and New Jersey.

Flooding impacts to urban areas are relatively minor, but indicate that airports, road systems, and low-lying coastal neighborhoods are most vulnerable. Impacted road systems are those most often located adjacent to larger water bodies or near dense agricultural regions where runoff from fields could cause pooling along roads. Finally, wind can exacerbate coastal marsh flooding by pushing water against the coastline (i.e., October 2019; July 2018 events).

B. Water Occurrence Discussion

The ability to isolate low occurrence waters from permanent water bodies becomes imperative in coastal flooding studies. An occurrence map allows permanent water bodies to be systematically removed from images of interest, rather than relying solely on a pre-post flood difference or manual extraction [50]. Studies that attempted to extract permanent water bodies often use the normalized difference water index on preflood SAR images [51]; however, using a single image to define permanent water is not always accurate considering WLs fluctuate with factors such as daily tidal cycles and wind speed, causing inherent pre- and postflood differences unrelated to storm flooding. Therefore, the use of an occurrence map provides a more accurate definition of permanent water since its definition is based on water information from multiple years rather than a single day. Moreover, an advantage of using an occurrence map is the ability to create a mask based on a user-defined definition of permanent water, $>$ 80% occurrence in this case, but can be modified for other applications depending on the focus.

C. Sensitivity Analysis of Tidal Water Levels

This section explores the importance of the maximum tidal extent product. Delaware Bay is a heavily tidally influenced region with WLs that fluctuate daily and result in temporary inundation primarily in coastal marshes (see Fig. 5). Removing these contributions from flood analysis is therefore essential since flood estimates could be over- or underestimated if the pre–post tidal amplitudes are different; meaning, the water left behind after the pre-post comparison could simply be a consequence of daily tidal fluctuations rather than storm-generated surge or precipitation. Using the maximum tidal extent product therefore improved flood estimates by removing tidal contributions from

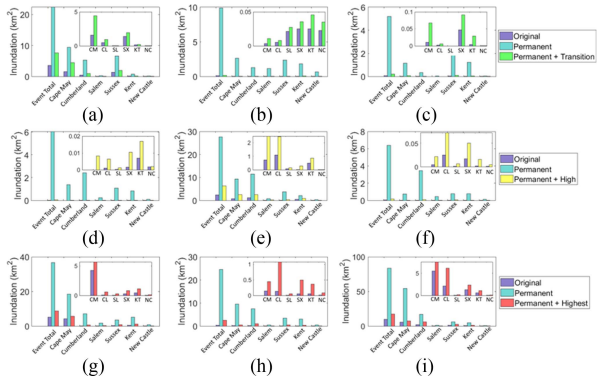

Fig. 14. Reanalysis of nine flood events three of which belong to the transition group with WL 0.1–1.0 m (a-c), three belong to the high group with WL 1.0–1.5 m (d-f), and three belong to the highest group with WL $>$ 1.5 m (g-i). Comparison between marsh estimates after removing maximum tidal extent (Original), permanent water only (Permanent), and permanent water plus specific tide mask (Permanent + Transition/High) are shown for each event. As many of the estimates are small, subsets are used to enlarge marsh estimates for Delaware Bay's six coastal counties abbreviated Cape May (CM), Cumberland (CL), Salem (SL), Sussex (SX), Kent (KT), New Castle (NC).

analysis. The importance of tidal removal can be further emphasized by repeating flood analysis on marsh estimates using the same methodology for flood detection, but without applying the maximum tidal extent product. Therefore, reanalyzed marsh estimates now include both tidal water and storm contributions. Marsh estimates were chosen for reanalysis since water within the maximum tidal extent product was primarily identified based on their marsh locations.

Analysis was performed using two different methods to reestimate marsh flooding. The same methodology was used for flood identification, except the maximum tidal extent product was replaced by either: 1) no maximum tidal extent product (referenced as the permanent method), or 2) a specialized tidal mask (referenced as the tidal method), where the specialized masks corresponded to different tidal stages. Reanalysis values from each method were compared to original marsh estimates.

To create these specialized tidal masks, the same nonstorm water maps used to create the maximum tidal extent product are divided into three categories based on WL to generate tidal maps. These maps are transition (WL 0.1–1.0 m), high (WL 1.0–1.5 m), and highest (WL $>$1.5 m). Categories are named based on the tidal stage present during image acquisition. Imagery in the transition category is named for imagery acquired during periods of tidal transition as water is entering or exiting Delaware Bay between high and low tide. This is followed by the high category named for those coinciding with high tide with WLs approximating mean high water; and finally, the highest category with images coinciding with the highest water levels in the Bay region which exceed MHHW (WL $>$ 1.5 m).

A composite of all imagery within each category is generated to create a spatial mask denoting the maximum tidal extent for each respective WL category. A composite of the transition, high, and highest water level masks match the maximum tidal extent mask.

Reanalysis results are shown in Fig. 14. Nine storm events were chosen for reanalysis, three events from each WL category.

Original marsh estimates (purple bars) are compared to marsh estimates computed without the use of the maximum tidal extent product (blue bars) or a specialized tidal mask (green, yellow, and red bars).

Overall, analysis highlights the importance of tidal removal from flood analysis as marsh estimates became notably larger, as seen by the several magnitudes increase if included in analysis (blue bars in Fig. 14). This could cause storm contributions to be considered significant based on total inundation, but this inundation might not solely be the result of the storm. Additionally, the use of tide-specific masks revealed that marshes are vulnerable to both tidal and storm inundation; however, this additional flooding is not significantly larger as reanalysis values and original estimates were typically within 0.5 km^2 of each other. The largest differences between original and reanalysis marsh values across both methods were contributed by primarily Cape May and Cumberland counties because they experience the largest tidal variability.

Results of both methods support the conclusion that using the maximum tidal extent product improves flood estimates in tidally influenced regions as it removes the variability associated with daily fluctuating WLs. However, method two highlights potential implications for using specialized tidal masks in regions where large tidal amplitudes and therefore additional marsh flooding could be more significant. It should be noted that the maximum tidal extent product removes any water within the range of tidal fluctuations, which can include floodwaters if a storm coincides with low tide. However, since this flooding is comparable to natural water level variations, it is likely occurring in regions expected to be inundated daily and therefore not the focus of this article.

VI. Conclusion

Flooding has become an increasing concern to coastal communities in recent years as climate change continues to modify environmental parameters, making it easier for more frequent and intense storms and therefore flooding to occur. The NE U.S. has been identified as particularly vulnerable, as this region is experiencing higher than average sea level rise rates, higher mean precipitation during storms, and increasing sunny-day flooding events. Regions around Delaware Bay are at high risk due to their flat topography, low mean elevation, and high land subsidence rates. SAR is a pivotal tool in observing Earth's surface features and, when combined with the power of deep learning, can provide insights into hazardous events like storm-induced flooding [52]. In this article, we trained the Modified DeepLabv3+ neural network to characterize coastal flooding around Delaware Bay between 2017 and 2021. Six Sentinel-1 VV-polarized GRD images were used to create a training dataset from which water labels were manually generated. The accuracy, precision, recall, dice coefficient, and mIoU of the model were 0.985, 0.987, 0.967, 0.977, and 0.966, respectively. Visualization of model performance confirms that the trained model can extract water bodies with clear and complete boundaries.

The trained model was used to generate water maps from 136 Sentinel-1 images of Delaware Bay between 2017 and 2021. To isolate storm-related floodwaters in 26 storm images, permanent water bodies and daily tidal inundation was systematically removed from imagery using water occurrence maps and a novel product referred to as maximum tidal extent. The presented methodology improves flood water estimates by focusing analysis on anomalously inundated regions impacted only by storm events.

Quantification of flood events reveal that most storms typically result in less than 2 km^2 per county, with Cumberland, Sussex, and Kent counties experiencing the most variability. Primary impacts were to agricultural regions in five of six counties, with Cape May dominated by marsh flooding. Minor urban flooding was observed and primarily impacted airport and road systems. Repeating analysis on marsh estimates revealed the importance of tidal removal from flooded imagery as the inclusion of tidal waters can lead to an increase in marsh estimates by several magnitudes. The use of specialized tidal masks revealed that additional marsh flooding is present within tidally inundated regions; however, estimates were typically within 0.5 km^2 of original marsh values, so using the maximum tidal extent product is supported in this region.

Case study analysis provided general characterizations about Delaware Bay flooding. First, extreme flooding events typically result from a combination of multiday precipitation and high water levels. These conditions can significantly impact agricultural areas across the entire region as well as coastal marsh locations. Single-day, intense precipitation can cause large areal flooding, but impacts mostly inland agricultural regions. Wind can exacerbate coastal flooding by pushing water toward the coastline, resulting in significant marsh flooding on one or both sides of the Bay. Although urban impacts are relatively small, the most flood prone and therefore vulnerable regions appear to be airports, low-lying neighborhoods adjacent to large, tidally influenced water bodies, as well as roads near these impacted urban centers. Additional case studies could be used to further expand upon these characterizations.

Overall, this study provided a baseline for flooding around Delaware Bay. It also introduced a novel methodology to improve coastal storm flood estimates in regions where pre–post differences are insufficient for flood analysis. The use of a tidal mask allows analysis to focus on regions impacted by storm conditions outside the natural variability of daily tidal cycles. Future analysis could explore regional sensitivity to flooding and why some regions are more flood prone. This could aid future mitigation efforts as climate change continues to modify the environment.

References

[1] S. Hallegatte, C. Green, R. J. Nicholls, and J. Corfee-Morlot, "Future flood losses in major coastal cities," *Nat. Climate Change*, vol. 3, no. 9, pp. 802–806, Sep. 2013, doi: 10.1038/nclimate1979.

[2] N. Beden and A. Ulke Keskin, "Flood map production and evaluation of flood risks in situations of insufficient flow data," *Nat. Hazards*, vol. 105, no. 3, pp. 2381–2408, Feb. 2021, doi: 10.1007/s11069-020-04404-y.

[3] H. Tabari, "Climate change impact on flood and extreme precipitation increases with water availability," *Sci. Rep.*, vol. 10, no. 1, Aug. 2020, Art. no. 13768, doi: 10.1038/s41598-020-70816-2.

[4] T. Ezer and L. P. Atkinson, "Accelerated flooding along the U.S. East Coast: On the impact of sea-level rise, tides, storms, the Gulf Stream, and the North Atlantic Oscillations," *Earths Future*, vol. 2, no. 8, pp. 362–382, 2014, doi: 10.1002/2014EF000252.

[5] W. V. Sweet et al., "Global and regional sea level rise scenarios for the United States: Updated mean projections and extreme water level probabilities along U.S. Coastlines," Nat. Ocean. Atmos. Administ., Silver Spring, MD, USA, Government Rep. NOS 01, Feb. 2022.

[6] M. Ghanbari, M. Arabi, S.-C. Kao, J. Obeysekera, and W. Sweet, "Climate change and changes in compound coastal-riverine flooding hazard along the U.S. Coasts," *Earths Future*, vol. 9, no. 5, 2021, Art. no. e2021EF002055, doi: 10.1029/2021EF002055.

[7] G. Boni et al., "A prototype system for flood monitoring based on flood forecast combined with COSMO-SkyMed and Sentinel-1 data," *IEEE J. Sel. Topics Appl. Earth Observ. Remote Sens.*, vol. 9, no. 6, pp. 2794–2805, Jun. 2016, doi: 10.1109/JSTARS.2016.2514402.

[8] S. Martinis et al., "Comparing four operational SAR-based water and flood detection approaches," *Int. J. Remote Sens.*, vol. 36, no. 13, pp. 3519–3543, Jul. 2015, doi: 10.1080/01431161.2015.1060647.

[9] A. M. Braga, R. C. P. Marques, F. A. A. Rodrigues, and F. N. S. Medeiros, "A median regularized level set for hierarchical segmentation of SAR images," *IEEE Geosci. Remote Sens. Lett.*, vol. 14, no. 7, pp. 1171–1175, Jul. 2017, doi: 10.1109/LGRS.2017.2702062.

[10] R. Bentivoglio, E. Isufi, S. N. Jonkman, and R. Taormina, "Deep learning methods for flood mapping: A review of existing applications and future research directions," *Hydrol. Earth Syst. Sci.*, vol. 26, no. 16, pp. 4345–4378, 2022, doi: 10.5194/hess-26-4345-2022.

[11] Z. Guo, L. Wu, Y. Huang, Z. Guo, J. Zhao, and N. Li, "Water-body segmentation for SAR images: Past, current, and future," *Remote Sens.*, vol. 14, no. 7, Jan. 2022, Art. no. 1752, doi: 10.3390/rs14071752.

[12] C. Liu, Y. Xiao, and J. Yang, "A coastline detection method in polarimetric SAR images mixing the region-based and edge-based active contour models," *IEEE Trans. Geosci. Remote Sens.*, vol. 55, no. 7, pp. 3735–3747, Jul. 2017.

[13] C. Liu, Y. Luo, J. Yang, and S. Wang, "Coastline detection in polarimetric SAR images based on Freeman decomposition and three-region Markov random field segmentation," *IEEE Geosci. Remote Sens. Lett.*, vol. 21, Jan. 2024, Art. no. 4002405.

[14] C. Sarker, L. Mejias, F. Maire, and A. Woodley, "Flood mapping with convolutional neural networks using spatio-contextual pixel information," *Remote Sens.*, vol. 11, no. 19, Jan. 2019, Art. no. 2331, doi: 10.3390/rs11192331.

[15] K. Khosravi et al., "Convolutional neural network approach for spatial prediction of flood hazard at national scale of Iran," *J. Hydrol.*, vol. 591, Dec. 2020, Art. no. 125552, doi: 10.1016/j.jhydrol.2020.125552.

[16] N. Kimura, I. Yoshinaga, K. Sekijima, I. Azechi, and D. Baba, "Convolutional neural network coupled with a transfer-learning approach for time-series flood predictions," *Water*, vol. 12, no. 1, Jan. 2020, Art. no. 96, doi: 10.3390/w12010096.

[17] B. Liu, X. Li, and G. Zheng, "Coastal inundation mapping from bitemporal and dual-polarization SAR imagery based on deep convolutional neural networks," *J. Geophys. Res. Oceans*, vol. 124, no. 12, pp. 9101–9113, 2019, doi: 10.1029/2019JC015577.

[18] B. Peng, Z. Meng, Q. Huang, and C. Wang, "Patch similarity convolutional neural network for urban flood extent mapping using bi-temporal satellite multispectral imagery," *Remote Sens.*, vol. 11, no. 21, Jan. 2019, Art. no. 2492, doi: 10.3390/rs11212492.

[19] J. A. Callahan, D. J. Leathers, and C. L. Callahan, "Comparison of extreme coastal flooding events between tropical and midlatitude weather systems in the Delaware and Chesapeake Bays for 1980–2019," *J. Appl. Meteorol. Climatol.*, vol. 61, no. 4, pp. 457–472, Apr. 2022, doi: 10.1175/JAMC-D-21-0077.1.

[20] H. Huang, H. Cui, and Q. Ge, "Assessment of potential risks induced by increasing extreme precipitation under climate change," *Nat. Hazards*, vol. 108, no. 2, pp. 2059–2079, Sep. 2021, doi: 10.1007/s11069-021-04768-9.

[21] E. Bevacqua et al., "More meteorological events that drive compound coastal flooding are projected under climate change," *Commun. Earth Environ.*, vol. 1, no. 1, Nov. 2020, Art. no. 47, doi: 10.1038/s43247-020-00044-z.

[22] A. Arns et al., "Non-linear interaction modulates global extreme sea levels, coastal flood exposure, and impacts," *Nat. Commun.*, vol. 11, no. 1, Apr. 2020, Art. no. 1918, doi: 10.1038/s41467-020-15752-5.

[23] Y. J. Zhang et al., "Simulating compound flooding events in a hurricane," *Ocean Dyn.*, vol. 70, no. 5, pp. 621–640, May 2020, doi: 10.1007/s10236-020-01351-x.

[24] J. A. Callahan, D. J. Leathers, and C. L. Callahan, "Skew surge and storm tides of tropical cyclones in the Delaware and Chesapeake Bays for 1980–2019," *Front. Climate*, vol. 3, 2021, Art. no. 610062.

[25] J. Yin, M. E. Schlesinger, and R. J. Stouffer, "Model projections of rapid sea-level rise on the northeast coast of the United States," *Nat. Geosci.*, vol. 2, no. 4, pp. 262–266, Apr. 2009, doi: 10.1038/ngeo462.

[26] M. A. Karegar, T. H. Dixon, and S. E. Engelhart, "Subsidence along the Atlantic Coast of North America: Insights from GPS and late holocene relative sea level data," *Geophys. Res. Lett.*, vol. 43, no. 7, pp. 3126–3133, 2016, doi: 10.1002/2016GL068015.

[27] D. Nikitina, A. C. Kemp, S. E. Engelhart, B. P. Horton, D. F. Hill, and R. E. Kopp, "Sea-level change and subsidence in the Delaware Estuary during the last ∼2200 years," *Estuarine, Coastal Shelf Sci.*, vol. 164, pp. 506–519, Oct. 2015, doi: 10.1016/j.ecss.2015.08.012.

[28] J. Boon, J. Brubaker, and D. Forrest, "Chesapeake bay land subsidence and sea level change : An evaluation of past and present trends and future outlook," Virginia Inst. Marine Sci., Gloucester Point, VA, USA, Y Rep. 425, Nov. 2010, doi: 10.21220/V58X4P.

[29] S. Li et al., "Evolving tides aggravate nuisance flooding along the U.S. coastline," *Sci. Adv.*, vol. 7, no. 10, Mar. 2021, Art. no. eabe2412, doi: 10.1126/sciadv.abe2412.

[30] P. A. Garzo and T. Fernández-Montblanc, "Land use/land cover optimized SAR coherence analysis for rapid Coastal disaster monitoring: The impact of the Emma storm in Southern Spain," *Remote Sens.*, vol. 15, no. 13, Jan. 2023, Art. no. 3233, doi: 10.3390/rs15133233.

[31] S. Radhika, Y. Tamura, and M. Matsui, "Cyclone damage detection on building structures from pre- and post-satellite images using wavelet based pattern recognition," *J. Wind Eng. Ind. Aerodyn.*, vol. 136, pp. 23–33, Jan. 2015, doi: 10.1016/j.jweia.2014.10.018.

[32] T. E. McKenna, "Characterization of tidal wetland inundation in the Murderkill estuary," Delaware Geological Survey, Newark, Delaware, Tech. Rep. 81, Mar. 2018.

[33] S. Lv, L. Meng, D. Edwing, S. Xue, X. Geng, and X.-H. Yan, "High-performance segmentation for flood mapping of HISEA-1 SAR remote sensing images," *Remote Sens.*, vol. 14, no. 21, Jan. 2022, Art. no. 5504, doi: 10.3390/rs14215504.

[34] K.-C. Wong and A. Münchow, "Buoyancy forced interaction between estuary and inner shelf: Observation," *Continental Shelf Res.*, vol. 15, no. 1, pp. 59–88, Jan. 1995, doi: 10.1016/0278-4343(94)P1813-Q.

[35] N. L. Jackson, "Wind and waves: Influence of local and non-local waves on mesoscale beach behavior in estuarine environments," *Ann. Assoc. Amer. Geographers*, vol. 85, no. 1, pp. 21–37, Mar. 1995, doi: 10.1111/j.1467-8306.1995.tb01793.xa.

[36] M. Salehi, "Storm surge and wave impact of low-probability hurricanes on the Lower Delaware Bay—Calibration and application," *J. Mar. Sci. Eng.*, vol. 6, no. 2, Jun. 2018, Art. no. 54, doi: 10.3390/jmse6020054.

[37] S. B. Lee, M. Li, and F. Zhang, "Impact of sea level rise on tidal range in Chesapeake and Delaware Bays," *J. Geophys. Res. Oceans*, vol. 122, no. 5, pp. 3917–3938, 2017, doi: 10.1002/2016JC012597.

[38] A. C. Ross, R. G. Najjar, M. Li, S. B. Lee, F. Zhang, and W. Liu, "Fingerprints of sea level rise on changing tides in the Chesapeake and Delaware bays," *J. Geophys. Res. Oceans*, vol. 122, no. 10, pp. 8102–8125, 2017, doi: 10.1002/2017JC012887.

[39] D. R. Smith, B. Lorne J., M. T. Mandt, and M. J. Millard, "Age and sex specific timing, frequency, and spatial distribution of horseshoe crab spawning in Delaware Bay: Insights from a large-scale radio telemetry array," *Curr. Zoology*, vol. 56, no. 5, pp. 563–574, Oct. 2010, doi: 10.1093/czoolo/56.5.563.

[40] J. T. Ellis and D. J. Sherman, "Chapter 1 - perspectives on coastal and marine hazards and disasters," in *Coastal and Marine Hazards, Risks, and Disasters* (Hazards and Disasters Series), J. F. Shroder, J. T. Ellis, and D. J. Sherman, Eds. Amsterdam, The Netherlands: Elsevier, 2015, pp. 1–13, doi: 10.1016/B978-0-12-396483-0.00001-7.

[41] R. G. Lathrop Jr, M. Allen, and A. Love, "Mapping and assessing critical horseshoe crab spawning habitats of Delaware Bay," Center Remote Sens. Spatial Analy., Rutgers University, New Brunswick, NJ, USA, Jul. 2006.

[42] M. S. Kearney et al., "Landsat imagery shows decline of coastal marshes in Chesapeake and Delaware Bays," *Eos, Trans. Amer. Geophysical Union*, vol. 83, no. 16, pp. 173–178, 2002, doi: 10.1029/2002EO000112.

[43] R. Stammermann and M. Piasecki, "Influence of sediment availability, vegetation, and sea level rise on the development of tidal marshes in the Delaware Bay: A review," *J. Coastal Res.*, vol. 28, no. 6, pp. 1536–1549, Nov. 2012, doi: 10.2112/JCOASTRES-D-11-00143.1.

[44] H. Stevens and A. Trembanis, "Stabilizing the forgotten Shore: Case study from the Delaware Bay," in *Pitfalls of Shoreline Stabilization: Selected Case Studies* (Coastal Research Library), J. A. G. Cooper and O. H. Pilkey, Eds.I Berlin, Germany: Springer-Verlag, 2012, pp. 267–281, doi: 10.1007/978-94-007-4123-2_16.

[45] A. Torralba, B. C. Russell, and J. Yuen, "LabelMe: Online image annotation and applications," *Proc. IEEE*, vol. 98, no. 8, pp. 1467–1484, Aug. 2010, doi: 10.1109/JPROC.2010.2050290.

[46] L. Yang et al., "A new generation of the United States National land cover database: Requirements, research priorities, design, and implementation strategies," *ISPRS J. Photogrammetry Remote Sens.*, vol. 146, pp. 108–123, Dec. 2018, doi: 10.1016/j.isprsjprs.2018.09.006.

[47] J. Wickham, S. V. Stehman, D. G. Sorenson, L. Gass, and J. A. Dewitz, "Thematic accuracy assessment of the NLCD 2016 land cover for the conterminous United States," *Remote Sens. Environ.*, vol. 257, May 2021, Art. no. 112357, doi: 10.1016/j.rse.2021.112357.

[48] L.-C. Chen, Y. Zhu, G. Papandreou, F. Schroff, and H. Adam, "Encoder-decoder with atrous separable convolution for semantic image segmentation," in *Proc. Comput. Vis., ECCV*, 2018, pp. 833–851. doi: 10.1007/978-3-030-01234-2_49.

[49] I. Olthof and T. Rainville, "Dynamic surface water maps of Canada from 1984 to 2019 Landsat satellite imagery," *Remote Sens. Environ.*, vol. 279, Sep. 2022, Art. no. 113121, doi: 10.1016/j.rse.2022.113121.

[50] M. R. Rahman and P. K. Thakur, "Detecting, mapping and analysing of flood water propagation using synthetic aperture radar (SAR) satellite data and GIS: A case study from the Kendrapara District of Orissa State of India," *Egyptian J. Remote Sens. Space Sci.*, vol. 21, pp. S37–S41, Jul. 2018, doi: 10.1016/j.ejrs.2017.10.002.

[51] J. J. Jesudasan, S. Saravanan, and D. Abijith, "Integration of SAR and multi-spectral imagery in flood inundation mapping – A case study on Kerala floods 2018," *ISH J. Hydraul. Eng.*, vol. 28, pp. 480–490, Nov. 2022, doi: 10.1080/09715010.2020.1791265.

[52] L. Meng et al., "Synthetic aperture radar for geosciences," *Rev. Geophys.*, vol. 62, 2024, Art. no. e2023RG000821.

Deanna Edwing received the B.S. degree in oceanography with a minor in geospatial technologies and the B.A. degree in geosciences with a minor in geology from the University of North Carolina Wilmington, Wilmington, NC, USA, both in 2021, and the M.S. degree in marine studies concentration in oceanography from the University of Delaware, Newark, DE, USA, in 2023.

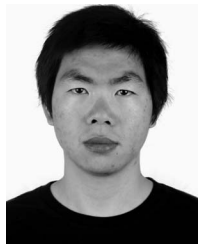

Lingsheng Meng received the bachelor's degree in marine fishery from Jimei University, Xiamen, China, in 2012, and the dual Ph.D. degree in oceanography from the University of Delaware, Newark, DE, USA, and Xiamen University, Xiamen, in 2022.

He is currently a Postdoctoral Researcher with the University of Delaware.

Suna Lv received the bachelor's degree in marine technology from Guangdong Ocean University, Zhanjiang, China, in 2019, and the master's degree in physical oceanography from Xiamen University, Xiamen, China, in 2022.

She is currently a Geomatics Assistant Engineer in Fuzhou, China.

Xiao-Hai Yan received the Ph.D. degree in satellite and physical oceanography from the State University of New York, Albany, NY, USA, in 1989.

He is currently a Professor with the University of Delaware, Newark, DE, USA. His research interests include physical oceanography, ocean remote sensing, climate change, air-sea interaction, ocean circulation, image processing, and environmental monitoring.